Biomaterials Science

PAPER

View Article Online
View Journal | View Issue

Cite this: *Biomater. Sci.*, 2017, **5**, 2169

pH and redox dual-sensitive polysaccharide nanoparticles for the efficient delivery of doxorubicin

Shengcai Yang,[a,b] Zhaohui Tang,[*b] Dawei Zhang,[b] Mingxiao Deng[c] and Xuesi Chen[a,b]

A pH and redox dual-sensitive biodegradable polysaccharide, succinic acid-decorated dextran-*g*-phenylalanine ethyl ester-*g*-cysteine ethyl ester (Dex-SA-L-Phe-L-Cys), was synthesized to load doxorubicin hydrochloride (DOX·HCl). The DOX-loaded nanoparticles, which were prepared in aqueous solution and free of organic solvent, could spontaneously self-assemble into uniform sizes. When loading DOX·HCl, mercapto Dex-SA-L-Phe-L-Cys was oxidized into a crosslinked disulfide linkage to form pH and redox dual-sensitive nanoparticles (DOX-S-NPs). The amphiphilic polymer loaded DOX·HCl into the core through electrostatic and hydrophobic interactions, meanwhile the crosslinked disulfide bond could stabilize the drug loaded nanoparticles. As a control with similar polymer structure, succinic acid decorated dextran-*g*-phenylalanine ethyl ester (Dex-SA-L-Phe) was prepared to obtain pH-sensitive DOX-loaded micelles (DOX-N-NPs). The controlled pH and redox-dependent release profiles of the DOX-S-NPs *in vitro* were certified in different releasing mediums. Furthermore, the cellular uptake of the DOX-S-NPs was comparable with that of free DOX·HCl, determined by confocal laser scanning microscopy (CLSM) and flow cytometry. Cytotoxicity assay *in vitro* showed that the DOX-S-NPs and free DOX·HCl were similar in inhibiting the proliferation of non-small cell lung carcinoma A549 and breast cancer MCF-7 cell lines. DOX-S-NPs displayed similar antitumor efficiency compared with free DOX·HCl, but lower toxicity by body weight. These dual-sensitive DOX-S-NPs provide a useful strategy for anti-tumor therapy.

Received 18th July 2017,
Accepted 31st August 2017

DOI: 10.1039/c7bm00632b

rsc.li/biomaterials-science

Introduction

Cancer has become an enormous threat to human health, resulting in ever-larger amounts of people dying every year.[1] Among the various tumor treatments, chemotherapy is one of the most common methods,[2,3] with doxorubicin hydrochloride (DOX·HCl), cisplatin (CDDP), and gemcitabine (GEM) being frontline clinical anticancer drugs.[4–6] However, the poor selectivity limits the application of chemotherapy.[7] The free drugs can enter not only tumor cells but also normal tissue cells, causing grave systemic toxicity and a poorly curative effect. To overcome the aforementioned problem, nanomedicine was put forward in the 1980s and developed rapidly in virtue of its special advantages.[8,9] Nano-carriers can efficiently load free drugs and circulate in the blood to avoid clearance by the renal and reticuloendothelial systems (RES), meanwhile dramatically enhancing the anticancer effect by accumulating in the tumor *via* the enhanced permeability and retention (EPR) effect and selectively releasing the cargo in the tumor sites.[10,11]

Doxorubicin hydrochloride (DOX·HCl), an anthracycline antibiotic, is one of the most dominating clinically-used anticancer drugs and possesses a wide spectrum of treatment possibilities.[4,12] DOX·HCl can embed in DNA or RNA, inhibit the synthesis of nucleic acids and effectively induce cell apoptosis.[13] However, the side effects of myelosuppression as well as cardiotoxicity severely limit its application and its hydrophilicity inhibits the drug loading efficiency.[14,15] Generally, for the preparation of DOX·HCl nanomedicine, DOX·HCl is neutralized with excess triethylamine to produce a hydrophobic form, doxorubicin.[16–19] The hydrophobic doxorubicin, dissolved in dimethyl sulfoxide (DMSO), *N*,*N*′-dimethyl formamide (DMF), dichloromethane or any other organic solvent rather than water, can be loaded by an amphiphilic copolymer through hydrophobic interaction. However, the organic solvent residual in the nanoparticles may be harmful to health, and in

[a]*College of Chemistry, Jilin University, Changchun, 130012, P. R. China*
[b]*Key Laboratory of Polymer Ecomaterials, Changchun Institute of Applied Chemistry, Chinese Academy of Sciences, Changchun, 130022, P. R. China.*
E-mail: ztang@ciac.ac.cn; Fax: +86-431-85262116; Tel: +86-431-85262116
[c]*College of Chemistry, Northeast Normal University, Changchun 130024, P. R. China*

addition the anticancer activity of the hydrophobic doxorubicin is reduced.[20]

The development of a smart amphiphilic copolymer, which is capable of accomplishing rapid drug release when arriving at the tumor sites and averting premature release of cargo in blood circulation,[21–26] has been a key issue in materials structure designing. In recent years, an increasing number of stimuli-sensitive smart nanoparticles were reported and these can release the cargos rapidly under certain stimuli (light, pH, temperature, glutathione, *etc.*).[27–31] For instance, utilizing the difference in the redox potential between an intracellular concentration of glutathione (GSH) and extracellular environment (~10 mM *vs.* ~2 μM), which is present even at higher levels in the cancer cells, a series of redox-sensitive polymers have been designed for controlled drug delivery *in vivo*.[32–36] In addition, various studies have confirmed that the pH in the intracellular environment of more aggressive tumor cells is lower than that of normal cells and normal blood systems.[37] Hence, it will be a promising and convenient design if a nano-carrier responds to two intrinsic stimuli (redox and pH) to control the payload release behaviors.[38]

Dextran is a natural analogue of poly(ethylene glycol) (PEG) with comprehensive applications in the biomedicine field owing to its outstanding aqueous solubility, biocompatibility and nontoxicity.[21,22,39,40] Herein, succinic acid decorated dextran (Dex-SA) was synthesized as a hydrophilic backbone with abundant carboxyl and hydroxyl groups. L-Phenylalanine ethyl ester hydrochloride (L-Phe) and L-cysteine ethyl ester hydrochloride (L-Cys) were elaborately introduced to serve as hydrophobic moieties and crosslinking points.[41,42] The prepared polymer Dex-SA-L-Phe-L-Cys, which is pH and redox-sensitive, can load DOX·HCl in an innocuous aqueous solution through electrostatic and hydrophobic interactions, meanwhile hydrosulphonyl can be oxidized into the disulfide bond to stabilize the micelle (DOX-S-NPs). In addition, Dex-SA-L-Phe with a similar polymer structure was prepared to obtain only pH-sensitive DOX-loaded micelles (DOX-N-NPs). The promising drug-loaded nanoparticles were assessed for their physicochemical characteristics, release behaviors, cellular uptake, cytotoxicity *in vitro* and antitumor efficacy *in vivo*.

Experimental section

Materials

Doxorubicin hydrochloride (DOX·HCl, Beijing Huafeng United Technology Corporation), *N*-hydroxysuccinimide (NHS, Aladdin), 1-(3-dimethylaminopropyl)-3-ethylcarbodiimide hydrochloride (EDCl, Aladdin), L-phenylalanine ethyl ester hydrochloride (L-Phe, Aladdin), L-cysteine ethyl ester hydrochloride (L-Cys, J&K chemical Ltd), 3-(4,5-dimethyl-thiazol-2-yl)-2,5-diphenyl tetrazolium bromide (MTT, Sigma) and 4′,6-diamidino-2-phenylindole dihydrochloride (DAPI, Sigma) were used as received without further purification. Dimethyl sulfoxide (DMSO) and triethylamine (Et_3N) were stored over calcium hydride (CaH_2) for 24 h and purified by vacuum distillation with CaH_2. All the other reagents were purchased from the Sinopharm Chemical Reagent Co. Ltd and used as received.

Methods

The ^1H NMR spectra were recorded on a Bruker AV 300 NMR spectrometer in D_2O. GPC analyses of Dex, Dex-SA, Dex-SA-L-Phe and Dex-SA-L-Phe-L-Cys were conducted on a Waters 2414 system equipped with an Ultra hydrogel linear column and a Waters 2414 refractive index detector (eluent: 0.1 M phosphate buffer, pH 7.4; flow rate: 0.5 mL min^{-1}; temperature: 35 °C; standard: poly(ethylene glycol)). The zeta potentials of the samples were measured by a Zeta Potential/BI-90Plus particle size analyzer (Brookheaven Instruments Corporation, USA). Dynamic laser scattering (DLS) measurement was performed on a WyattQELS instrument with a vertically polarized HeNe laser (Dawn EOS, Wyatt Technology, USA). The scattering angle was fixed at 90°. The critical micelle concentration (CMC) was measured by fluorescence spectroscopy using Nile Red as a probe on a PerkinElmer LS50B luminescence spectrometer with an emission wavelength of 550 nm. The UV–Vis spectra were measured on a UV-2401PC spectrophotometer (SHIMADZU). Elemental analysis was accomplished using a Varian EL microanalyzer.

The synthesis of Dex-SA-L-Phe and Dex-SA-L-Phe-L-Cys

The synthesis of Dex-SA was conducted according to our previous work.[22] To prepare Dex-SA-L-Phe-L-Cys, Dex-SA (1.00 g, 3.08 mmol –COOH) and anhydrous DMSO (15.0 mL) were added to a 100 mL dried flask and heated to 50 °C in an oil bath until Dex-SA dissolved. When the above solution had cooled to room temperature, EDCl (124 mg, 0.646 mmol) and NHS (68.0 mg, 0.592 mmol) were added, followed by three freeze–thaw cycles and activation overnight. Under the protection of argon, L-Phe (107 mg, 0.462 mmol) and L-Cys (14.3 mg, 0.0769 mmol) were added and Et_3N (0.0624 mL, 0.538 mmol) was injected *via* a syringe. All the reaction procedures were conducted in water-free and argon conditions, and the reaction was proceeded for 48 h at room temperature (RT). The crude products were precipitated in cooled ethanol, filtered, washed 3 times with ethanol and dried under vacuum at RT. The crude products were redissolved in deionized water, dialyzed (MWCO 3500) against deionized water for 3 days and then freeze-dried to give Dex-SA-L-Phe-L-Cys. As a control compound, the synthesis of Dex-SA-L-Phe was similar, the differences were the dosage of EDCl (106 mg, 0.554 mmol), NHS (58.4 mg, 0.508 mmol), L-Phe (107 mg, 0.462 mmol) and Et_3N (0.0535 mL, 0.462 mmol) and the process of deoxygenation was also omitted.

The synthesis of DOX-N-NPs and DOX-S-NPs

Dex-SA-L-Phe-L-Cys (87.0 mg) was dissolved in distilled water (10.0 mL), the pH adjusted to 7.4, and 3.0 mL of distilled water solution of DOX·HCl (15.9 mg) was added to this solution dropwise. The above liquid was stirred overnight, dialyzed (MWCO 3500) against deionized water for 1 day, filtered through a 0.45 μm pore-sized microporous membrane, and

freeze-dried to obtain DOX-S-NPs. The DOX-N-NPs were prepared similarly with Dex-SA-L-Phe instead of Dex-SA-L-Phe-L-Cys. All these operations were conducted under darkness. The change in the particle size of the developed nanoparticles in 10% (v/v) FBS solution was monitored by DLS for 84 h. The drug loading content (DLC) and drug loading efficiency (DLE) of the DOX-NPs were determined using UV-Vis spectroscopy at 488 nm using the following calculation formulae:

$$\text{DLC\%} = \frac{\text{weight of DOX loaded in nanoparticles}}{\text{weight of DOX-loaded nanoparticles}} \times 100\%$$

$$\text{DLE\%} = \frac{\text{weight of DOX loaded in nanoparticles}}{\text{weight of feeding DOX}} \times 100\%$$

The release of DOX·HCl *in vitro*

To investigate the release behavior of DOX-S-NPs, the weighted freeze-dried nanoparticles were dissolved in 5 mL of phosphate buffered saline (PBS) solution of various pH values (7.4, 6.5, or 5.2) or 20 mM GSH in PBS (pH 7.4) and transferred into a dialysis bag (MWCO 3500 Da). Then the release assays were initiated by adding 25 mL of homologous PBS into the outer dialysis bag of a 37 °C shaking box (100 rpm) under darkness. At predetermined time points, 10 mL of the release solution was withdrawn with the same volume of fresh PBS supplemented. The amount of DOX·HCl in the release media was determined using UV-Vis spectroscopy at 488 nm. Similarly, the release profiles of DOX·HCl in the DOX-N-NPs were conducted in PBS (pH 7.4, 6.5 or 5.2) without GSH.

Cell culture

The non-small cell lung cancer (A549) cells and breast cancer (MCF-7) cells were purchased from Shanghai Bogoo Biotechnology Co. Ltd. The cells were cultured in Dulbecco's modified Eagle's medium (DMEM, Gibco) with high glucose containing 10% fetal bovine serum (FBS), supplemented with 1% penicillin and 1% streptomycin and incubated at 37 °C in a 5% CO_2 atmosphere.

Cellular uptake

The celluar uptake was determined by flow cytometry and confocal laser scanning microscopy (CLSM).

For the flow cytometry assay, 3×10^5 MCF-7 cells per well were seeded in the 6-well plate and incubated overnight with 2 mL of DMEM, and then replaced with fresh DMEM containing DOX·HCl, DOX-N-NPs or DOX-S-NPs (at a final DOX·HCl concentration of 5 mg mL^{-1}). After 1 h and 3 h, the cells were washed 3 times with 3 mL of PBS, treated by trypsin without EDTA and collected in 1 mL of PBS. The cell suspension was centrifuged at 900 rpm for 5 min and washed twice with 1 mL of PBS. Eventually, the cells were suspended in 0.3 mL of PBS for flow cytometry tests (BD Biosciences, CA, USA).

For the CLSM assay, 10^5 MCF-7 cells per well were seeded onto glass coverslips placed in the 6-well plate and incubated overnight for a cell adherence culture with 2 mL of DMEM, then replaced with fresh DMEM with DOX·HCl, DOX-N-NPs or DOX-S-NPs (at a final DOX·HCl concentration of 5 mg mL^{-1}). After 1 h and 3 h, the cells were washed 3 times with 3 mL of PBS and fixed with 4% formaldehyde for 20 min at room temperature, followed by washing the residual formaldehyde 3 times with 3 mL of PBS. According to the manufacturer's instructions, the cell nuclei were stained with DAPI. The coverslips were placed onto glass microscope slides and fixed with nail polish, and the cellular uptake of DOX·HCl was visualized using a CLSM (Carl Zeiss LSM 700).

Cellular cytotoxicity assay *in vitro*

To verify the biocompatibility of Dex-SA-L-Phe and Dex-SA-L-Phe-L-Cys, two different cell lines, MCF-7 and A549, were used. The MCF-7 or A549 cells were seeded in the 96-well plates with a density of 7000 cells per well and incubated overnight with 100 μL of DMEM for the cell adherence culture, then replaced with 200 μL of fresh DMEM with different concentrations of Dex-SA-L-Phe and Dex-SA-L-Phe-L-Cys. The cells were subjected to MTT assay after being incubated for another 24 h. Specifically, at the end of the experiments, 20 μL of MTT (1 mg mL^{-1} in sterile PBS) was added into the 96-well plates for another 4 h of incubation. The supernatant was removed and 100 μL of DMSO was added. The absorbance of the solution was measured on a Bio-Rad 680 microplate reader at 490 nm. The relative cell viability (%) was calculated by the following formula:

$$\text{Cell viability } (\%) = (A_{\text{experimental}}/A_{\text{control}}) \times 100$$

$A_{\text{experimental}}$ and A_{control} represent the absorbance of the experimental well and control well, respectively. The data are presented as the average ± SD (n = 3).

The cellular cytotoxicities of DOX·HCl, the DOX-N-NPs and DOX-S-NPs were also validated by MTT assay. The MCF-7 or A549 cells were seeded in 96-well plates, 7000 cells per well, and different concentrations of free DOX·HCl, DOX-N-NPs and DOX-S-NPs were added for 24 or 48 h of incubation, to confirm the time and dose-dependence of the DOX·HCl and DOX nanoparticles.

Animals

Female Balb/C nude mice (6–8 weeks old) were obtained from the Beijing Vital River Laboratory Animal Technology Co., Ltd (Beijing, China). The mice were raised in a specific pathogen free (SPF) animal lab. All the animals received care in compliance with the guidelines outlined in the Guide for the Care and Use of Laboratory Animals and all procedures were approved by the Animal Care and Use Committee of Jilin University.

Antitumor efficiency *in vivo*

MCF-7 cells (2×10^6 per mouse) were subcutaneously injected into the right mammary fat pad to obtain the orthotopic breast xenograft tumor model. The mice were divided into

4 groups randomly when the tumor volume reached approximately 50 mm^3. The 4 groups of mice were treated with PBS (control), free DOX·HCl (3 mg kg^{-1}), DOX-N-NPs (3 mg kg^{-1} on DOX·HCl basis) or DOX-S-NPs (3 mg kg^{-1} on DOX·HCl basis) and injected intravenously *via* the tail vein on day 0, 4, 7, and 10. The antitumor activity was evaluated by the tumor volume (V_t), tumor-growth-rate (TGR) and tumor-suppress-rate (TSR), which were calculated using the following equations. Meanwhile, the body weight was measured simultaneously every other day as a symbol of the systemic toxicity. At the end of the assay, the mice were sacrificed. The tumors and major organs (heart, liver, spleen, lung and kidney) were excised for histopathology analyses.

$$\text{Tumor volume } (V_t, \text{mm}^3) = a \times b^2/2$$

$$\text{Tumor-growth-rate } (\text{TGR}, \%) = (V_t/V_0) \times 100\%$$

$$\text{Tumor-suppress-rate } (\text{TSR}, \%) = [(\text{TGR}_c - \text{TGR}_x)/\text{TGR}_c] \times 100\%$$

a and b represent the longest and shortest diameters of the tumors, measured by a vernier caliper, respectively. V_0 represents the tumor volume on day 0. Subscript c and x represent the control group and treatment group, respectively.

Histological and immunohistochemical analyses

The excised tumors and major organs were fixed in 4% PBS buffered paraformaldehyde overnight, and then embedded in paraffin. The paraffin embedded tumors and organs were cut at a 5 μm thickness and stained with hematoxylin and eosin (H&E) to assess the histological alterations using an optical microscope (Nikon TE2000U).

Statistical analysis

All experiments were performed at least three times and expressed as the mean ± SD. The data were analyzed for statistical significance using the Student's *t*-test. $p < 0.01$ was considered a significant difference.

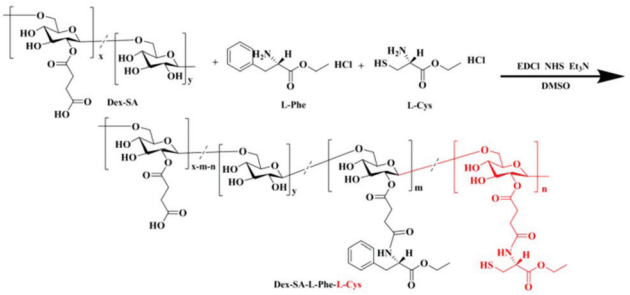

Scheme 1 The synthesis of Dex-SA-L-Phe-L-Cys.

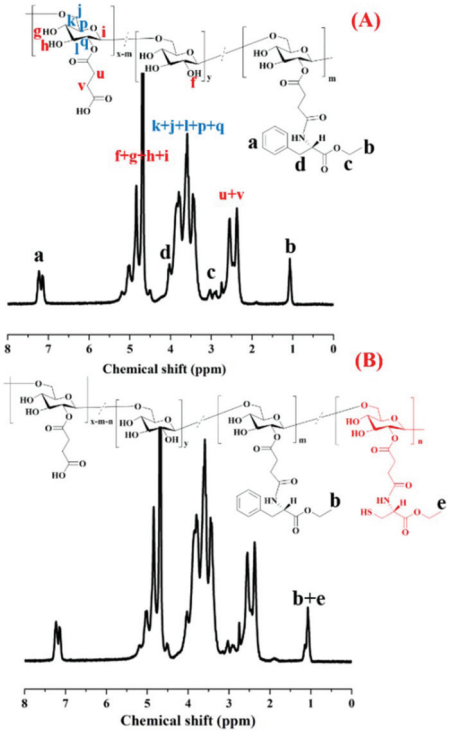

Fig. 1 The ^{1}H NMR spectra of Dex-SA-L-Phe (A) and Dex-SA-L-Phe-L-Cys (B) in D_2O.

Results and discussion

The synthesis of Dex-SA-L-Phe and Dex-SA-L-Phe-L-Cys

The synthesis of Dex-SA-L-Phe-L-Cys is shown in Scheme 1. Dex-SA was synthesized according to our previous work and subsequently conjugated with L-Phe and L-Cys to form side chains and obtain Dex-SA-L-Phe-L-Cys.

The ^{1}H NMR spectra of Dex-SA-L-Phe and Dex-SA-L-Phe-L-Cys are shown in Fig. 1. For Dex-SA-L-Phe (Fig. 1A), the signals of C_6H_5– (a) and $–CH_2CH_3$ (b) in the L-Phe unit are at δ 7.17–7.29 and 1.11 ppm, respectively. Similarly, for Dex-SA-L-Phe-L-Cys (Fig. 1B), the signals δ 1.07–1.14 ppm are $–CH_2CH_3$ in the L-Phe unit (b) and L-Cys unit (e). As our previous work showed, the number of SA units per 100 anhydroglucosidic units was 50, so we determined that x and y were 50.[22] Verified by the elemental analysis, the amounts of the L-Phe and L-Cys units in Dex-SA-L-Phe-L-Cys are 19 and 4 while the control material Dex-SA-L-Phe contains 19 L-Phe groups. The GPC analyses (Fig. 2 and Table 1) show that the number average molecular weights (M_n) of Dex-SA-L-Phe-L-Cys and Dex-SA-L-phe are 23.8×10^3 and 23.7×10^3, while the poly dispersity indexes (PDI, M_w/M_n) are 2.36 and 2.42. All these results confirm the successful conjugation of the hydrophobic and crosslinking groups with Dex-SA.

The critical micelle concentration (CMC) was measured by fluorescence spectroscopy using Nile red as a probe. Briefly, 25 mg of Dex-SA-L-Phe-L-Cys was dissolved in 5 mL of millQ-water, and 1 mL of Nile red solution (1 mM Nile red in DMF) was added under gentle stirring. After stirring overnight, the mixed solution was dialyzed against distilled water for 24 h and diluted with water to 10 mL. Then, the sample was double

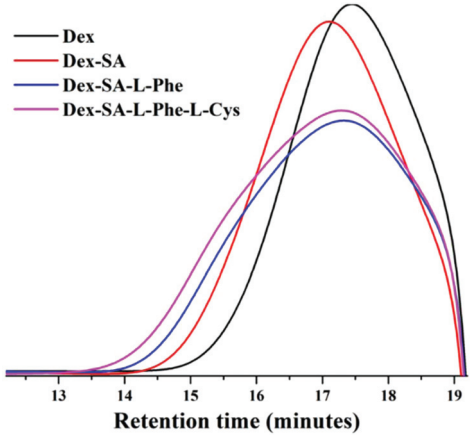

Fig. 2 The GPC traces of Dex, Dex-SA, Dex-SA-L-Phe and Dex-SA-L-Phe-L-Cys.

Table 1 The characterization of the blank nanoparticles

Entry	R_h [a]/nm	Zeta potential[b]/mV	CMC[c]/ mg L^{-1}	$M_n \times 10^{-3}$/ g mol^{-1}	PDI
Dex-SA-L-Phe	21.4 ± 4.13	−6.89 ± 0.95	6.5	23.7	2.36
Dex-SA-L-Phe-L-Cys	20.4 ± 5.35	−8.76 ± 1.33	4.6	23.8	2.42

[a] Measured by DLS at 25 °C. [b] Estimated at pH 7.4 at 25 °C, the mean ± SD of 7 measurements. [c] Determined by fluorescence spectroscopy.

diluted in turn to measure using fluorescence spectroscopy. The Dex-SA-L-Phe-L-Cys blank nanoparticles have an extremely low CMC, 4.6 mg L^{-1} (Table 1), indicating that the nanoparticles possess great stability against immense dilution. Because of the crosslinked disulfide bond, the Dex-SA-L-Phe-L-Cys blank nanoparticles have a smaller CMC than the Dex-SA-L-phe blank nanoparticles, 6.5 mg L^{-1}. Such a low CMC value will ensure that the micelles maintain their spherical construct throughout the diluted conditions (*e.g.* blood stream) *in vivo*, which is a great benefit for effective drug delivery to tumors.

The synthesis and characterization of the DOX-loaded nanoparticles

The smart pH and redox dual-responsive Dex-SA-L-Phe-L-Cys was designed to load hydrophilic free drug DOX·HCl. The preparation of the DOX-loaded nanoparticles was conducted in an aqueous medium without any organic solvent, which was convenient and nontoxic. In practical terms, the pH of the Dex-SA-L-Phe-L-Cys solution was adjusted to 7.4 to guarantee that the carboxyl group deprotonated completely. Furthermore, the DOX-S-NPs were prepared in an open beaker to ensure that the sulfhydryl group oxidized into a disulfide bond. The DOX-S-NPs were formed through self-assembly between the hydrophobic L-Phe segment and hydrophobic DOX, and at the same time stabilized by the electrostatic interactions of the carboxylic acid ion. Moreover, the polymer had a sulfhydryl group (–SH) as a crosslinking point to keep the nanoparticles stable in normal conditions (*e.g.* blood system) and sensitive in the reduced conditions (*e.g.* tumor intracellular environment).

The DOX-S-NPs were pH and redox dual-sensitive nanoparticles, while the DOX-N-NPs were only pH-sensitive. The DOX-N-NPs were obtained using a pH-sensitive material, Dex-SA-L-Phe, which has abundant carboxyl and hydrophobic moieties (L-Phe). Dex-SA-L-Phe could load DOX·HCl innocuously into the aqueous solution through electrostatic and hydrophobic interactions.

The DLC and DLE of the DOX-S-NPs were 13.0% and 84.7% (Table 2), respectively, denoting the successful loading of DOX·HCl. The size distribution of the DOX-S-NPs was measured by DLS. As shown in Fig. 3A and Table 2, the nanoparticles had a radius of about 62.7 nm, which could escape liver, spleen and RES clearances and accumulate into the tumors by the EPR effect. The zeta potential of the DOX-S-NPs was −6.61 mV and the weakly negative surface charge facilitates the lengthening circulation of the nanoparticles.

Similarly, the DLC and DLE values of the DOX-N-NPs were 13.4% and 86.7%, respectively (Table 2). The DOX-N-NPs exhibited analogous hydrodynamic radius and zeta potential, *i.e.* 63.5 nm and −5.57 mV, which were almost the same as those of the DOX-S-NPs, avoiding the interference of the particle size and potential in treatment.

The serum stability of the nanoparticles was investigated by co-incubation with 10% FBS. The DOX-N-NPs stayed stable for 12 h, but a slight size increase was detected after 24 h of incubation (Fig. 3B). However, the DOX-S-NPs kept a constant size in FBS for 84 h, which indicated that they were stable under physiological conditions due to their lower affinity for plasma

Table 2 The characterization of the DOX-loaded nanoparticles

Entry	R_h [a]/nm	DLC[b]/%	DLE/%	Zeta potential[c]/mV
DOX-N-NPs	63.5 ± 14.8	13.4	86.7	−5.57 ± 1.48
DOX-S-NPs	62.7 ± 15.9	13.0	84.7	−6.61 ± 1.45

[a] Measured by DLS at 25 °C. [b] Determined by UV–Vis spectroscopy at 488 nm. [c] Estimated at pH 7.4 at 25 °C, the mean ± SD of 7 measurements.

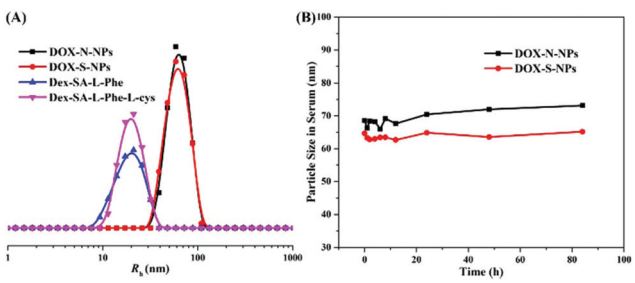

Fig. 3 The hydrodynamic radius distribution of the blank micelles and DOX-loaded nanoparticles in aqueous solution as determined by DLS (A). The change in the particle size (nm) of the DOX-loaded nanoparticles in serum for 84 h (B).

proteins. Therefore, the crosslinked DOX-S-NPs were more stable and could reach the tumor region without aggregation or precipitation in the blood stream.

The release behavior of the DOX-loaded nanoparticles

The *in vitro* release profiles of the pH and redox dual-sensitive DOX-S-NPs were studied in different PBS solutions (pH 7.4, 6.5 or 5.2) and PBS (pH 7.4) with 20 mM GSH. PBS environments with various pH values were used to testify the pH-sensitivity: (1) normal blood (pH 7.4); (2) tumor extracellular fluid (pH 6.5); (3) tumor endosome (pH 5.2).[43,44] As shown in Fig. 4B, the DOX·HCl cumulative releases within 24 h at pH values of 5.2, 6.5 and 7.4 were 76.2%, 50.2% and 27.8%, respectively, indicating that the more acidic environments contributed to faster release rates. The acidic environments boosted the protonation degree of the carboxyl groups, resulting in extensive disruption of their electrostatic interactions with DOX, meanwhile enhancing the hydrophilicity of DOX to accelerate the release behavior. But when 20 mM GSH was added into PBS (pH 7.4) to simulate the redox environments of the tumor cells, the DOX-S-NPs released almost 69.4% DOX·HCl within 24 h (Fig. 4C), confirming the redox-responsive release property of the DOX-S-NPs. Due to the lower pH and higher GSH concentration in the solid tumor intracellular environment,[45] the pH and redox dual-sensitive DOX-S-NPs could effectively reduce the undesired drug loss during blood circulation and preferentially release the drugs under tumor-relevant conditions after the accumulation at the tumor site through the ERP effect, leading to enhanced antitumor efficacy.

Similarly, approximately 70.5%, 50.0% and 29.6% of total DOX·HCl were released from the DOX-N-NPs within 24 h at pH values of 5.2, 6.5 and 7.4 (Fig. 4A), revealing the sensitivity under acid-biased pH stimuli.

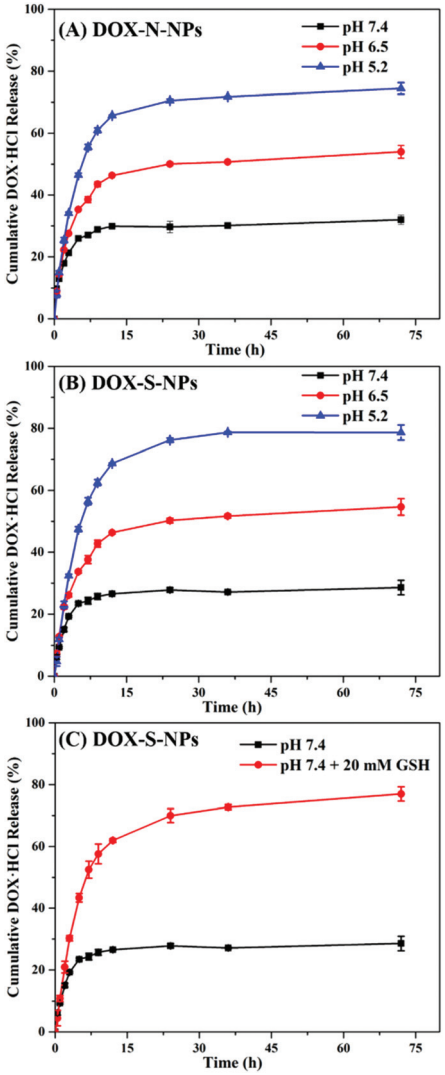

Fig. 4 The *in vitro* DOX·HCl release profiles of DOX-N-NPs (A) and DOX-S-NPs (B) in PBS with different pH values, and the DOX-S-NPs (C) in PBS (pH 7.4) with or without GSH.

Cellular uptake

The cellular internalizations of free DOX·HCl, the DOX-N-NPs or DOX-S-NPs were investigated by flow cytometry after incubation with the MCF-7 cells at 37 °C for 1 or 3 h. Since DOX·HCl possesses spontaneous red fluorescence, the DOX-NPs did not require labelling by any other luminescent dyes. The fluorescence intensity was positively correlated with the cellular uptake of DOX·HCl in the tumor cells. As Fig. 5 shows, in the MCF-7 cell lines, the DOX·HCl fluorescence intensity was increased through the lengthening of the incubation time from 1 h to 3 h, indicating that the behavior of the cellular uptake was time-dependent. And the fluorescence intensity of the DOX-N-NPs or DOX-S-NPs had no significant difference, implying that the DOX-NPs could release DOX·HCl rapidly after internalizing into the MCF-7 cells, which was also the same as DOX·HCl.

Similarly, the behaviors of the cellular uptake and DOX distribution were further determined by CLSM in the MCF-7 cells. The cell nuclei were stained blue with DAPI. Red fluorescence imaging was carried out to visualize DOX·HCl. Red fluorescence was observed in the cell nuclei after 1 h of incubation with DOX·HCl or the DOX-NPs and enhanced when the incubation time was extended to 3 h (Fig. 6). These phenomena manifested that the DOX-NPs could be internalized into the MCF-7 cells and release DOX·HCl in the cytoplasm, which can then rapidly enter the nucleus. Although free DOX·HCl and DOX-NPs could both be taken in by cancer cells, free DOX·HCl entered the cell by passive transport through the cell mem-

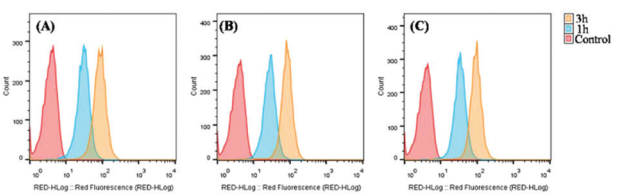

Fig. 5 The flow cytometric images of the MCF-7 cells after incubation with DOX·HCl (A), DOX-N-NPs (B) and DOX-S-NPs (C) for 1 h or 3 h.

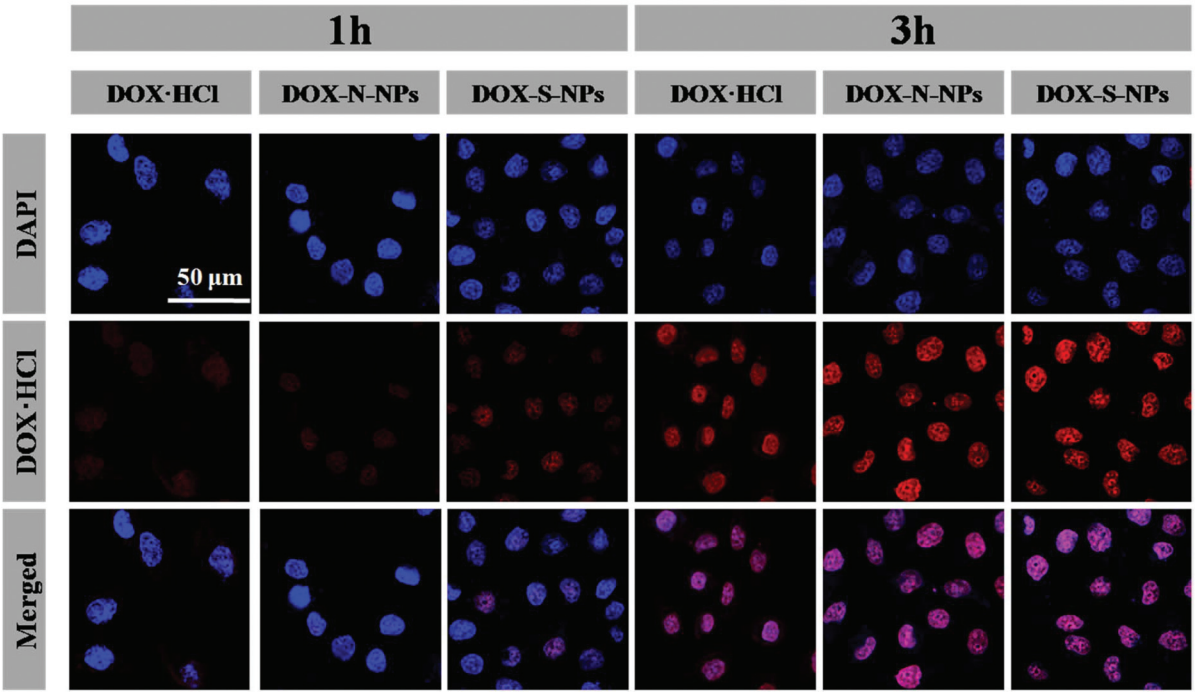

Fig. 6 The CLSM images of MCF-7 after incubation with DOX·HCl, DOX-N-NPs and DOX-S-NPs for 1 h or 3 h. Scale bar: 50 μm.

brane, while the DOX-NPs relied on the conventional endocytic pathways. The fluorescence intensities of free DOX·HCl and the DOX-NPs were almost identical, revealing that the velocity of the cellular uptake and release behavior of the DOX-NPs in the MCF-7 cell lines were comparable with free DOX·HCl.

Cell cytotoxicity

Firstly, the biocompatibilities of the Dex-SA-L-Phe and Dex-SA-L-Phe-L-Cys blank nanoparticles were verified by MTT assay using the MCF-7 and A549 cell lines. As shown in Fig. 7, the relative cell viability was almost above 80% after 24 h of incubation, even at a concentration of the blank nanoparticles up to 1 mg mL^{-1}, indicating the safety and excellent biocompatibility of the polysaccharide materials.

The antitumor activities of the non-crossed-linked DOX-N-NPs and crossed-linked DOX-S-NPs were conducted in the MCF-7 and A549 cells. The DOX-S-NPs could play an efficient role in inhibiting the cell viability, close to the cancer killing potency of DOX·HCl and the DOX-N-NPs (Fig. 8). The cell viabilities of both the MCF-7 and A549 cell lines treated with DOX·HCl, DOX-N-NPs or DOX-S-NPs were dose-dependent and time-dependent. For example, the IC_{50} values of DOX·HCl, the DOX-N-NPs and DOX-S-NPs observed in MCF-7 at 48 h were 0.49, 0.62 and 0.53 μg mL^{-1} (Table 3), respectively, indicating that the cancer killing potency of DOX·HCl and the DOX-NPs

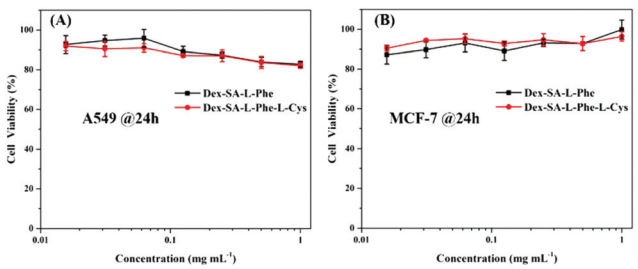

Fig. 7 The *in vitro* cytotoxicity of Dex-SA-L-Phe and Dex-SA-L-Phe-L-Cys to the A549 (A) and MCF-7 (B) cells at 24 h.

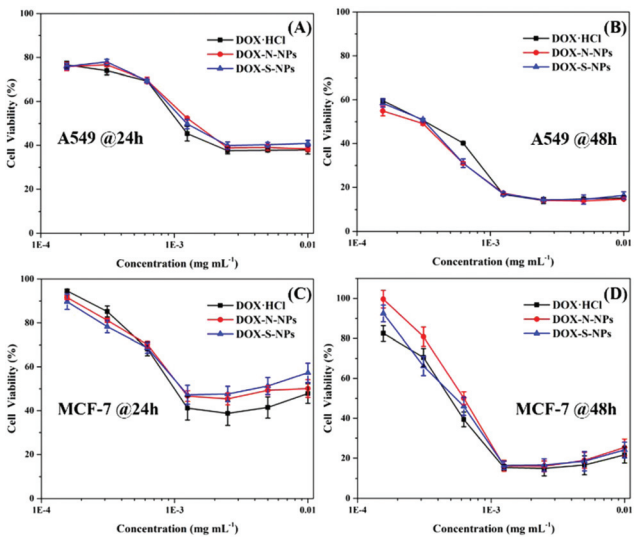

Fig. 8 The *in vitro* cell viabilities of the MCF-7 and A549 cells incubated with DOX·HCl, DOX-N-NPs and DOX-S-NPs for 24 h and 48 h.

Table 3 The IC_{50} of DOX·HCl, DOX-N-NPs and DOX-S-NPs on the MCF-7 and A549 cells at 24 h and 48 h

		MCF-7-IC_{50}/μg mL^{-1}	A549-IC_{50}/μg mL^{-1}
24 h	DOX·HCl	1.03	1.14
	DOX-N-NPs	1.27	1.40
	DOX-S-NPs	1.27	1.31
48 h	DOX·HCl	0.49	0.32
	DOX-N-NPs	0.62	0.25
	DOX-S-NPs	0.53	0.29

was coincident, and this was in agreement with the consequence of cellular uptake.

In vivo anticancer efficacy

Inspired by the excellent anti-proliferation effect of the DOX-NPs *in vitro*, the antitumor efficacy and systemic toxicity of the micelles on an MCF-7 orthotopic breast xenograft tumor model were conducted. When the tumors were about 50 mm^3, the mice received the treatment *via* intravenous injection with PBS, free DOX·HCl, DOX-N-NPs or DOX-S-NPs on days 0, 4, 7 and 10. The tumor volumes and mice body weights were measured every other day. As shown in Fig. 9A, compared with the control group, the mice treated with different DOX formulations showed remarkable inhibition of tumor growth. However, the free DOX·HCl treated mice started dying around day 10 and only 3 mice survived to day 14. The tumor-suppress-rates (TSR, %) of the DOX-N-NPs and DOX-S-NPs treated groups were 60% and 78%, respectively (Table 4 and Fig. 9C).

The changes of the mice's body weights were a symbol of the systemic toxicity. Fig. 9B showed that the free DOX·HCl treated mice had an overt body weight loss (nearly 25%), whereas the DOX-S-NPs treated mice had a relatively inconspicuous body weight change. The mice of the DOX-N-NPs group also had an obvious body weight loss (nearly 20%), indicating that the nanoparticles without –SH to act as a cross-linking point were less stable than the DOX-S-NPs, and this was tentatively attributed to immature release occurring during blood circulation, which was consistent with the results of the serum stability. The increased antitumor efficacy and decreased systemic toxicity of the DOX-S-NPs were potentially caused by the crosslinking stability, prolonged circulation time and sudden drug release in tumor sites.

Histological and immunohistochemical analyses

At the end of the antitumor experiments, to further assess the therapeutic effect of DOX·HCl and the DOX-NPs, the tumors and major organs were collected and stained with H&E for pathological analysis. For the H&E staining, the tumor treated with PBS had large nuclei and more chromatin, revealing the powerful ability of tumor cell proliferation (Fig. 10). In contrast, for different drug formulation treated groups, the tumor slices did not have normal and clear cell morphology, and the chromatin was concentrated and pyknotic or absent outside the cell. The degrees of tumor tissue necrosis treated with different DOX formulation were comparable, whereas there

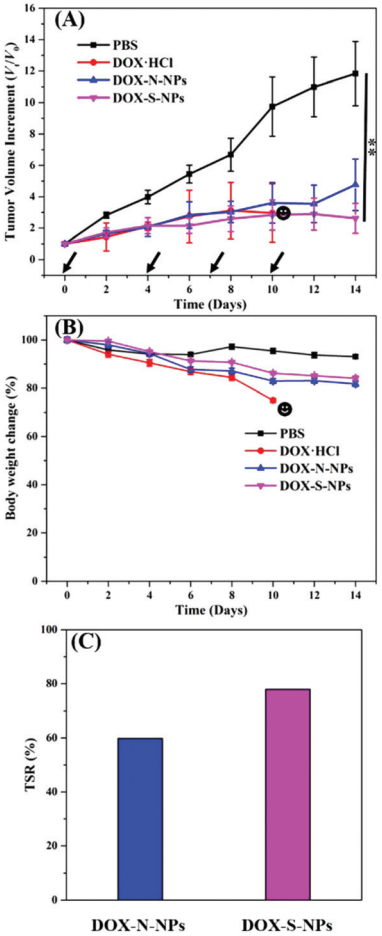

Fig. 9 The *in vivo* antitumor efficacy of DOX·HCl (3 mg kg^{-1}), the DOX-N-NPs (3 mg kg^{-1} DOX·HCl eq.) and DOX-S-NPs (3 mg kg^{-1} DOX·HCl eq.) in the MCF-7 tumor bearing Balb/C nude mice. (A) The tumor volume increment during the treatment. The black arrows represent the treatment day. (B) The body weight changes of the MCF-7 tumor bearing mice during the treatment. (C) The tumor-suppress-rate (TSR, %) of the DOX-N-NPs and DOX-S-NPs treated groups on day 14. The data are shown as mean ± SD (n = 7). The black face icon represents the free DOX·HCl treated mice that started dying on day 10. **p < 0.01.

Table 4 The tumor-growth-rate (TGR, %) and tumor-suppress-rate (TSR, %) of the PBS, DOX·HCl, DOX-N-NPs and DOX-S-NPs treated groups on day 14

	PBS	DOX·HCl	DOX-N-NPs	DOX-S-NPs
V_0 (mm^3)	49 ± 15	49 ± 11	37 ± 11	55 ± 15
V_{14} (mm^3)	580 ± 81	—	176 ± 35	143 ± 26
TGR (%)	1184	—	476	262
TSR (%)	—	—	60	78

was no obvious necrosis or significant morphological changes of the spleen, lung and kidney derived from mice in treatment groups compared to the control group. However, overtly varying degrees of damage of the heart and liver were observed in groups treated with free DOX·HCl and the DOX-N-NPs. Cardiotoxicity is a well-known side effect of free DOX·HCl in a

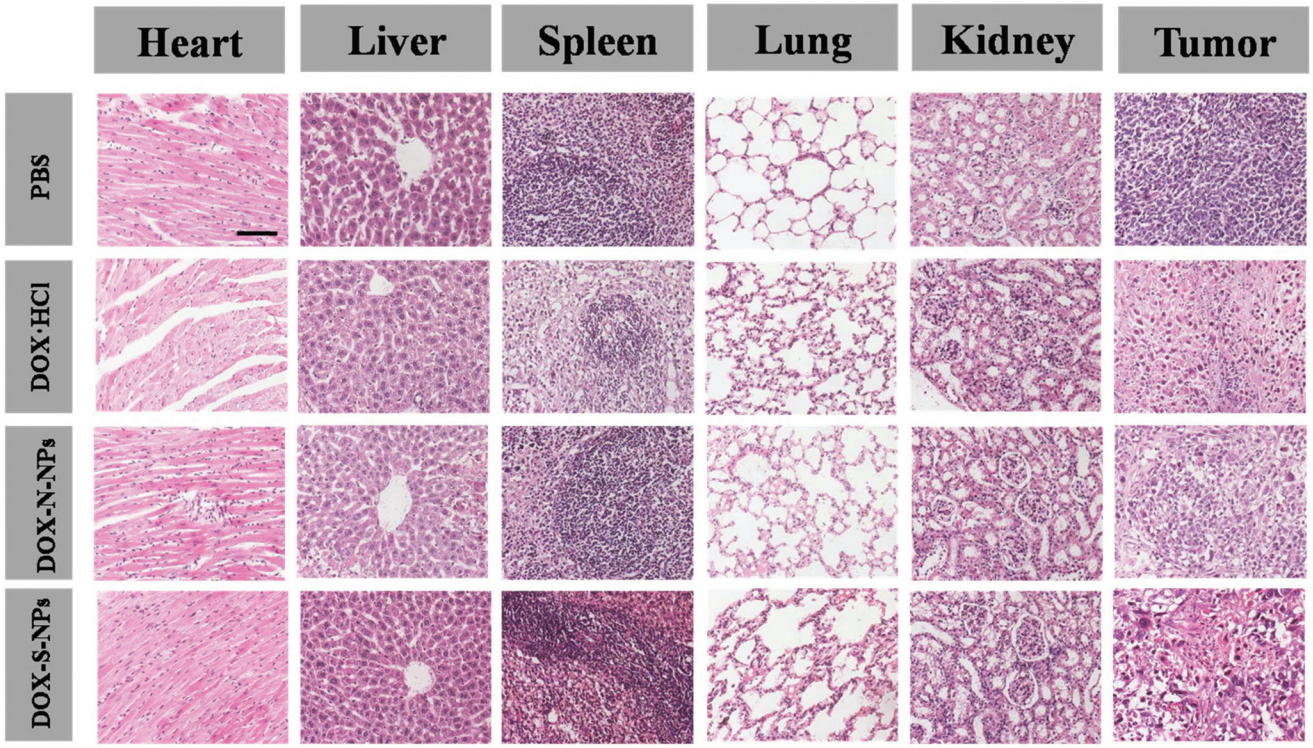

Fig. 10 Histologic assessments of major organs and tumors with H&E staining in the MCF-7 tumor bearing Balb/C nude mice. Scale bar: 200 μm.

clinical application.[46] Significant histological changes and necrosis of the muscle fibers of heart tissues were observed in free DOX·HCl and the DOX-N-NPs treated group. The obvious necrosis of hepatocytes was also observed in the DOX-N-NPs treated group, which was attributed to the accumulation of nanoparticles in the liver tissue, while the damage degree of the liver tissues was more moderate in the free DOX·HCl treated group. In contrast, the pathological images of the cardiac and liver tissues treated with crosslinked DOX-S-NPs had no difference from the control group.

Conclusions

We have developed a pH and redox dual-sensitive polysaccharide-based polymer, Dex-SA-L-Phe-L-Cys, to act as a smart nano-vehicle for loading a cationic and hydrophilic drug, DOX·HCl. The Dex-SA-based polymer possessed favorable biocompatibility and size distribution. The dual-sensitive DOX-loaded nanoparticles are stable under a normal physiological environment, but release cargo rapidly under weak acidic conditions and a reducing environment. The cytotoxicity of DOX-S-NPs in the MCF-7 and A549 cells *in vitro* was comparable to free DOX·HCl. For the *in vivo* antitumor efficacy of breast cancer MCF-7, DOX-S-NPs exhibited excellent antitumor activity and lower systemic toxicity than free DOX·HCl. Furthermore, the customized polymer, Dex-SA-L-Phe-L-Cys, can expand more widely for the delivery of other drugs.

Conflicts of interest

There are no conflicts of interest to declare.

Acknowledgements

This research was financially supported by the National Natural Science Foundation of China (Projects 51520105004, 51673189, 51473029, 51528303, 51390484, 51403204 and 51503202), Ministry of Science and Technology of China (Project 2017zx09101005-012), Science and Technology Service Network Initiative (Project KFJ-SW-STS-166) and Chinese Academy of Sciences Youth Innovation Promotion Association.

Notes and references

1 R. L. Siegel, K. D. Miller and A. Jemal, *CA-Cancer J. Clin.*, 2016, **66**, 7–30.
2 R. Siegel, D. Naishadham and A. Jemal, *CA-Cancer J. Clin.*, 2013, **63**, 11–30.
3 Y. Zhou, J. Song, L. Wang, X. Xue, X. Liu, H. Xie and X. Huang, *Biomacromolecules*, 2017, **18**, 2446–2453.
4 O. Tacar, P. Sriamornsak and C. R. Dass, *J. Pharm. Pharmacol.*, 2013, **65**, 157–170.
5 D. Lebwohl and R. Canetta, *Eur. J. Cancer*, 1998, **34**, 1522–1534.

6 D. Li, K. Xie, R. Wolff and J. L. Abbruzzese, *Lancet*, 2004, **363**, 1049–1057.
7 H. M. Kieler-Ferguson, J. M. J. Frechet and F. C. Szoka Jr., *Wiley Interdiscip. Rev.: Nanomed. Nanobiotechnol.*, 2013, **5**, 130–138.
8 D. Peer, J. M. Karp, S. Hong, O. C. FaroKhzad, R. Margalit and R. Langer, *Nat. Nanotechnol.*, 2007, **2**, 751–760.
9 R. Duncan, *Nat. Rev. Cancer*, 2006, **6**, 688–701.
10 T. Sun, Y. S. Zhang, B. Pang, D. C. Hyun, M. Yang and Y. Xia, *Angew. Chem., Int. Ed.*, 2014, **53**, 12320–12364.
11 H. Maeda, *Adv. Drug Delivery Rev.*, 2015, **91**, 3–6.
12 H. T. Ta, C. R. Dass, I. Larson, P. F. M. Choong and D. E. Dunstan, *Biomaterials*, 2009, **30**, 3605–3613.
13 K. Ueda, C. Cardarelli, M. M. Gottesman and I. Pastan, *Proc. Natl. Acad. Sci. U. S. A.*, 1987, **84**, 3004–3008.
14 S. Mazzucchelli, M. Bellini, L. Fiandra, M. Truffi, M. A. Rizzuto, L. Sorrentino, E. Longhi, M. Nebuloni, D. Prosperi and F. Corsi, *Oncotarget*, 2017, **8**, 8383.
15 M. Fojtu, J. Gumulec, T. Stracina, M. Raudenska, A. Skotakova, M. Vaculovicova, V. Adam, P. Babula, M. Novakova and M. Masarik, *Curr. Drug Metab.*, 2017, **18**, 237–263.
16 W. Xu, I. A. Siddiqui, M. Nihal, S. Pilla, K. Rosenthal, H. Mukhtar and S. Gong, *Biomaterials*, 2013, **34**, 5244–5253.
17 C.-y. Long, M.-m. Sheng, B. He, Y. Wu, G. Wang and Z.-w. Gu, *Chin. J. Polym. Sci.*, 2012, **30**, 387–396.
18 L. J. Zhang, B. Wu, W. Zhou, C. X. Wang, Q. Wang, H. Yu, R. X. Zhuo, Z. L. Liu and S. W. Huang, *Biomater. Sci.*, 2016, **5**, 98–110.
19 B. Wu, P. Yu, C. Cui, M. Wu, Y. Zhang, L. Liu, C. X. Wang, R. X. Zhuo and S. W. Huang, *Biomater. Sci.*, 2015, **3**, 655–664.
20 X. Xu, Y. Li, H. Li, R. Liu, M. Sheng, B. He and Z. Gu, *Small*, 2014, **10**, 1133–1140.
21 Y.-L. Li, L. Zhu, Z. Liu, R. Cheng, F. Meng, J.-H. Cui, S.-J. Ji and Z. Zhong, *Angew. Chem., Int. Ed.*, 2009, **48**, 9914–9918.
22 M. Li, Z. Tang, S. Lv, W. Song, H. Hong, X. Jing, Y. Zhang and X. Chen, *Biomaterials*, 2014, **35**, 3851–3864.
23 Y. Wu, W. Chen, F. Meng, Z. Wang, R. Cheng, C. Deng, H. Liu and Z. Zhong, *J. Controlled Release*, 2012, **164**, 338–345.
24 J. Dai, S. Lin, D. Cheng, S. Zou and X. Shuai, *Angew. Chem., Int. Ed.*, 2011, **50**, 9404–9408.
25 Y. Zhang, T. Ren, J. Gou, L. Zhang, X. Tao, B. Tian, P. Tian, D. Yu, J. Song, X. Liu, Y. Chao, W. Xiao and X. Tang, *J. Controlled Release*, 2017, **261**, 352–366.
26 Z. Tang, C. He, H. Tian, J. Ding, B. S. Hsiao, B. Chu and X. Chen, *Prog. Polym. Sci.*, 2016, **60**, 86–128.
27 C. Y. Ang, S. Y. Tan, C. Teh, J. M. Lee, M. F. Wong, Q. Qu, L. Q. Poh, M. Li, Y. Zhang, V. Korzh and Y. Zhao, *Small*, 2017, **13**, 1602379.
28 L. Nuhna, N. Vanparijs, A. D. Beuckelaer, L. Lybaert, G. Verstraete, K. Deswarte, S. Lienenklaus, N. M. Shukla, A. C. D. Salyer, B. N. Lambrecht, J. Grooten, S. A. David, S. D. Koker and B. G. D. Geest, *Proc. Natl. Acad. Sci. U. S. A.*, 2016, **113**, 8098–8103.
29 W. Wei, X. Zhang, X. Chen, M. Zhou, R. Xu and X. Zhang, *Nanoscale*, 2016, **8**, 8118–8125.
30 H. J. Li, J. Z. Du, X. J. Du, C. F. Xu, C. Y. Sun, H. X. Wang, Z. T. Cao, X. Z. Yang, Y. H. Zhu, S. Nie and J. Wang, *Proc. Natl. Acad. Sci. U. S. A.*, 2016, **113**, 4164–4169.
31 X. An, A. Zhu, H. Luo, H. Ke, H. Chen and Y. Zhao, *ACS Nano*, 2016, **10**, 5947–5958.
32 J. J. Mieyal, M. M. Gallogly, S. Qanungo, E. A. Sabens and M. D. Shelton, *Antioxid. Redox Signaling*, 2008, **10**, 1941–1988.
33 S. Lv, Z. Tang, D. Zhang, W. Song, M. Li, J. Lin, H. Liu and X. Chen, *J. Controlled Release*, 2014, **194**, 220–227.
34 J. Lee, E. T. Oh, H. Yoon, H. Kim, H. J. Park and C. Kim, *Nanoscale*, 2016, **8**, 8070–8077.
35 B. Cheng, B. Thapa, K. C. Remant and P. Xu, *J. Mater. Chem. B*, 2015, **3**, 25–29.
36 K. C. Rement, B. Thapa and P. Xu, *Mol. Pharm.*, 2012, **9**, 2719–2729.
37 S. K. Parks, J. Chiche and J. Pouyssegur, *J. Cell. Physiol.*, 2011, **226**, 299–308.
38 Z. Cai, H. Zhang, Y. Wei, Y. Wei, Y. Xie and F. Cong, *Biomacromolecules*, 2017, **18**, 2102–2117.
39 F. Zhang, S. Gong, J. Wu, H. Li, D. Oupicky and M. Sun, *Biomacromolecules*, 2017, **18**, 1793–1802.
40 Y. Zhang, L. Liu, T. Wang, H. Tian and X. Chen, *Acta Polym. Sin.*, 2017, **7**, 1150–1158.
41 Y. Zheng, Y. Yuan, Y. Chai and R. Yuan, *Biosens. Bioelectron.*, 2016, **79**, 86–91.
42 H. Yi, L. Liu, N. Sheng, P. Li, H. Pan, L. Cai and Y. Ma, *Biomacromolecules*, 2016, **17**, 1737–1747.
43 M. Kanamala, W. R. Wilson, M. Yang, B. D. Palmer and Z. Wu, *Biomaterials*, 2016, **85**, 152–167.
44 G. Moku, S. K. Gulla, N. V. Nimmu, S. Khalid and A. Chaudhuri, *Biomater. Sci.*, 2016, **4**, 627–638.
45 P. Kuppusamy, H. Li, G. Ilangovan, A. J. Cardounel, J. L. Zweier, K. Yamada, M. C. Krishna and J. B. Mitchell, *Cancer Res.*, 2002, **62**, 307–312.
46 J. L. Quiles, J. R. Huertas, M. Battino, J. Mataix and M. C. Ramirez-Tortosa, *Toxicol.*, 2002, **180**, 79–95.